ACS APPLIED NANO MATERIALS

Article

Cite This: ACS Appl. Nano Mater. 2020, 3, 195−206

www.acsanm.org

Mesoporous Silica−Gelatin Aerogels for the Selective Adsorption of Aqueous Hg(II)

Petra Herman,[†,‡] István Fábián,[†,§] and József Kalmár*[,†]

[†]Department of Inorganic and Analytical Chemistry and [‡]Doctoral School of Chemistry, University of Debrecen, Egyetem tér 1, Debrecen H-4032, Hungary

[§]MTA-DE Redox and Homogeneous Catalytic Reaction Mechanisms Research Group, Egyetem tér 1, Debrecen H-4032, Hungary

Supporting Information

ABSTRACT: Supercritically dried, mesoporous silica−gelatin hybrid aerogels of 4−24 wt % gelatin content show high selectivity for the adsorption of aqueous Hg(II) in the simultaneous presence of Cu(II), Cd(II), Co(II), Pb(II), Ni(II), Ag(I), and Zn(II), as demonstrated by batch adsorption experiments with multiple competing ions. The aerogels are characterized by SEM and N_2 porosimetry, and their aqueous particle size distributions and zeta potentials are reported. The adsorption properties of the hybrid aerogels are studied as a function of their composition, initial aqueous Hg(II) concentration, contact time, and pH. The optimum pH for adsorption is 6.0, where the surface of the aerogel is already negatively charged, but Hg(II) does not completely hydrolyze. The Hg(II) uptake of the hybrid aerogels increases with increasing gelatin content and levels off at 24 wt % gelatin. The adsorption capacity of the 24 wt % gelatin hybrid is estimated to be S = 209 mg g^{-1} by fitting the isotherm with the Langmuir model (K_L = 0.032 L mg^{-1}). This translates to 91% Hg(II) removal at c_0(Hg) = 1.0 mg L^{-1} and c_0(aerogel) = 0.32 g L^{-1}. Gelatin provides the active sites for Hg(II) binding; thus, higher gelatin content results in higher adsorption capacity. However, high gelatin content also induces the extensive swelling of backbone and the partial collapse of the open porous structure, which decreases the specific surface area. Time-resolved experiments show that the adsorption equilibrium is established within 15 min contact time with aqueous Hg(II). Washing the equilibrated aerogels with a 2.5 mM solution of EDTA complexing agent quantitatively liberates bound Hg(II). The regenerated aerogels demonstrate practically intact adsorption capacities in five cycles of reuse. Coordination chemistry based considerations reveal that Hg(II) is selectively complexed by the soft Lewis-base side chains of collagen.

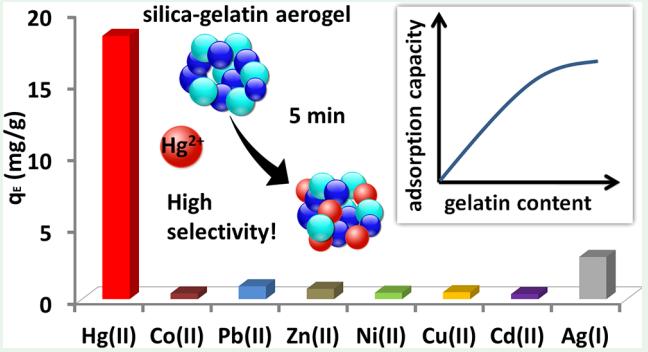

KEYWORDS: *aerogel, hybrid material, mercury, selective adsorption, natural water*

1. INTRODUCTION

The detection and removal of aqueous heavy metal ions is of outmost importance in chemical research and development.[1−3] Several technologies are implemented for the immobilization of heavy metal compounds, such as ion exchange, flocculation, membrane filtration, adsorption, and chemical precipitation.[4−6] From these methods, adsorption technologies are the most commonly used ones because of their cost-effectiveness and ease of operation.[7,8]

Aqueous mercury(II) [Hg(II)] is especially interesting from both the environmental and analytical points of view due to its high toxicity, diverse redox, coordination and organometallic chemistry, and its ability to form volatile compounds. A large variety of high performance and selective adsorbents have been developed in the past decade for the immobilization of aqueous Hg(II). The most promising advanced materials are solid, highly porous, functionalized adsorbents. One strategy for the preparation of these advanced materials is to fabricate selective, high affinity (e.g., sulfur containing) active sites for binding Hg(II) onto porous, inert supports (e.g., silica).[9−16] Another strategy is to synthesize superior composite or hybrid materials from natural Hg(II) adsorbents to enhance their performance and/or technical applicability. A frequently utilized, versatile component is chitosan.[17−22] Other versatile platforms are graphene and graphene oxide.[23−30] Porous synthetic polymers form the basis of exceptionally high durability adsorbents.[31−35] Magnetic particles are also frequently used platforms for advanced adsorbents because these particles can easily and selectively be separated from the liquid phase.[36−39] Composite preparations are also synthesized from gelatin, an archetypical biomaterial that has a well-known affinity toward Hg(II).[40−42] Most recently, the best overall adsorption performance has been reported for functionalized and hybrid porous graphene adsorbents, (e.g., cysteine and

Received: October 2, 2019
Accepted: December 24, 2019
Published: December 24, 2019

DOI: 10.1021/acsanm.9b01903
ACS Appl. Nano Mater. 2020, 3, 195−206

Scheme 1. Illustration of the Preparation and the General Structure of the Silica–Gelatin Hybrid Aerogels[a]

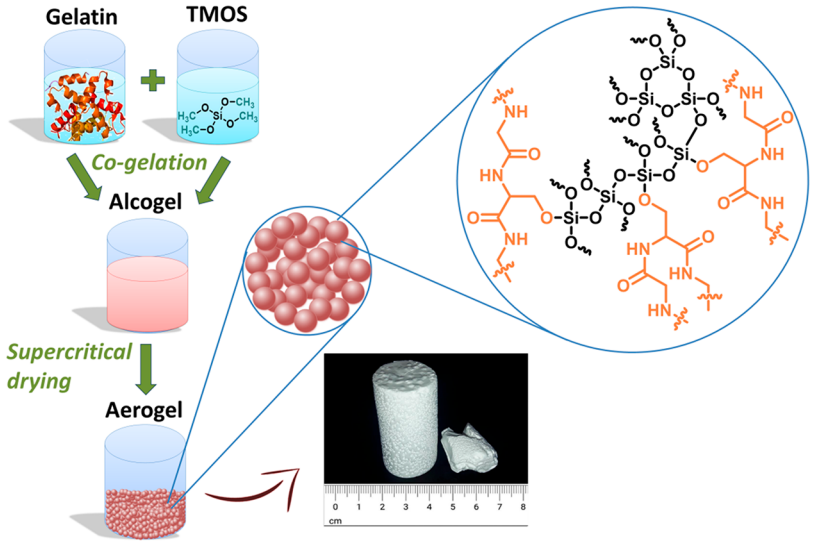

[a]The side chains of the serine and the threonine amino acids of gelatin are proposed to form covalent bonds linking the protein to the SiO_2 network.[56,57] The hybrid backbone forms primary globules ($d_{globule}$ = 50–100 nm) that are the main structural elements of the aerogel monoliths (cf. section 3.1.1).

αFeOOH decorated graphene and graphene oxide) and quantum dot or graphene decorated porous silica. Typically, these materials exhibit adsorption capacities between 100 and 800 mg g^{-1} at initial Hg(II) concentrations [c_0(Hg)] between 1.0 and 500 mg L^{-1} at adsorbent concentrations between 10 and 500 mg L^{-1}. In these systems, the adsorption equilibrium optimally completes in 60 min.[27,28,43,44]

Supercritically dried aerogels can be prepared from various starting materials. Hybrid and composite inorganic, organic, and biopolymer based aerogels are common for the past decade.[45] Silica, resorcinol–formaldehyde, and carbon aerogels functionalized by S, N, O, and P containing chelating groups are high performance adsorbents for aqueous heavy metal ions; thus, a large variety of adsorbents have recently been developed on aerogel platforms.[16,42,46–50] Supercritically dried aerogel adsorbents usually show superior adsorption characteristics due to their open mesoporous structures when benchmarked against freeze-dried cryogel adsorbents of the same base material and functionalization. This has been pointed out by recent critical reviews.[2,47,49,51]

In this study, we aimed to prepare gelatin containing aerogels with open mesoporous structures for the adsorption of aqueous Hg(II). For this reason, silica–gelatin hybrid gels of 4–24 wt % gelatin content were synthesized by the sol–gel method and dried by using supercritical CO_2 to obtain aerogels. These aerogels were designed by considering that the silica constituent provides high porosity, while the gelatin constituent ensures the affinity of the hybrids toward Hg(II). The as-prepared aerogels were characterized by scanning electron microscopy (SEM) and N_2 gas adsorption–desorption porosimetry. Adsorption experiments were conducted with aqueous Hg(II), Cu(II), Cd(II), Co(II), Pb(II), Ni(II), Ag(I), and Zn(II) at different pH values. To find the most important factors affecting the adsorption features of silica–gelatin aerogels, the thermodynamic and kinetic properties were correlated to the structural characteristics of the hybrids of different compositions. The size distribution and the zeta potential of the aerogels were taken into account for mechanistic considerations.[52,53]

2. EXPERIMENTAL SECTION

2.1. Materials and Solutions. All common solid ($(NH_4)_2CO_3$, $HgCl_2$, $K_2Cr_2O_7$, $Cu(NO_3)_2{\cdot}3H_2O$, $CdN_2O_6{\cdot}4H_2O$, $Co(NO_3)_2{\cdot}6H_2O$, $Pb(NO_3)_2$, $AgNO_3$, $Ni(NO_3)_2{\cdot}6H_2O$, $Zn(CH_3COO)_2{\cdot}2H_2O$, $FeCl_3{\cdot}6H_2O$, NaCl, EDTA, NaOH) and liquid (HNO_3, H_2O_2, HF, NH_3, CH_3OH, C_3H_6O) chemicals were ACS reagent grade (Sigma-Aldrich) and used without further purification. All aqueous solutions were prepared with ultrafiltered water (ρ = 18.2 MΩ cm by Milli-Q from Millipore). Tetramethyl orthosilicate (TMOS) was purchased from Fluka. Household gelatin (type A, 150 kDa, food grade) was obtained from Dr. Oetker because of the high and constantly guaranteed quality of the product. Supercritical CO_2 was produced from 99.5+% pure gas (Linde).

A Metrohm 888 Titrando automatic titrator unit equipped with a double-junction 6.0255.100 pH electrode was used to measure the pH values of the solutions. The desired pH was set by adding appropriate amounts of HNO_3 or NaOH solutions. Because heavy metal ions may form Cl^- precipitates and complexes, common single junction electrodes containing KCl electrolyte could not be used for this study. To avoid reactions between the electrode filling solution and the aqueous heavy metal ions, the above-mentioned double junction electrode, which has an additional salt bridge and an outer electrolyte of KNO_3, was applied.

2.2. Preparation of Silica–Gelatin Hybrid Aerogels. Silica–gelatin hybrid aerogels of varying gelatin content were synthesized by the sol–gel technique using the recipe reported previously.[53,54] The hybrid backbone was produced by a cogelation method. First, a solution was prepared by dissolving a given amount (from 0.10 to 0.60 g) of gelatin and 70.0 mg of $(NH_4)_2CO_3$ in 20.0 g of hot water. A second solution containing 3.30 g of tetramethyl orthosilicate (TMOS) and 5.55 g of MeOH was prepared. After cooling the gelatin solution near room temperature, the two solutions were mixed by vigorous stirring. The mixture was poured into a cylindrical plastic mold for gelation and was kept there for 24 h. The alcogel was removed from the mold and transferred into a perforated aluminum container for performing multistep solvent exchange. First, the sample was soaked in methanol for 24 h to remove water. Next, methanol was gradually replaced with acetone in four steps, each taking 24 h. Acetone was replaced two more times for fresh acetone every 24 h.

DOI: 10.1021/acsanm.9b01903
ACS Appl. Nano Mater. 2020, 3, 195–206

Finally, acetone was extracted with liquid CO_2 at 5.4 MPa at room temperature. The extensive solvent exchange ensures the excellent batch-by-batch reproducibility of both the microscopic and the macroscopic structures of the final aerogels. This is complemented by aging before supercritical drying to establish the completion of all secondary chemical processes.

The gel was dried with supercritical CO_2 at 14 MPa and 80 °C by using the medium-pressure technique, as reported previously.[55] Four types of hybrid aerogels were produced by this recipe that contain 4, 11, 18, or 24 wt % gelatin by dry weight. According to our experience, there is an elevated risk for the formation of local inhomogeneities in the aerogel backbone during synthesis above 24 wt % gelatin content; thus, hybrids of higher gelatin content were not prepared. The gelatin-free parent silica aerogel was prepared by the same recipe, but without the addition of gelatin to the aqueous $(NH_4)_2CO_3$ solution.

The preparation and the general structure of the silica−gelatin hybrid aerogels are illustrated in Scheme 1. It has recently been verified by solid-state NMR that during the cogelation (hydrolysis and polycondensation) of a tetraalkyl orthosilicate (e.g., TEOS and TMOS) and a protein, the −OH side chains of the threonine and serine amino acids of the protein react with the SiO_2 precursor orthosilicate and form −Si−O−C− covalent bonds. These primary bonds are the main reason for the high stability of the hybrid SiO_2−protein backbones.[56,57]

The gelatin contents of the dry, hybrid aerogels were measured by thermogravimetry, as reported previously.[54] The measured gelatin contents of the aerogels are practically the same as the values calculated based on the recipes. Gelatin does not leech into water during a week long soaking of the aerogels, indicating the stable incorporation of the protein into the backbone. Preliminary small-angle neutron scattering (SANS) experiments prove that the hybridization of the backbone is homogeneous at the molecular level. (The extensive discussion of the SANS characterization results of the silica−gelatin aerogels is out of the scope of the present article and will be published in the future.)

2.3. Aerogel Characterization. Scanning electron microscopic (SEM) images were recorded on a Hitachi S-4300 instrument (Hitachi Ltd., Tokyo, Japan). Aerogel shards, freshly split from the monoliths, were immobilized on carbon tapes, or embedded in Wood's metal, and covered by 5−6 atomic layer thick sputtered gold conductive layers. Typically, a 5−15 kV accelerating voltage was used. Electron microscopic images were evaluated by using NI Vision Assistant software (National Instruments, USA).

Specific surface areas, pore size distributions, and total pore volumes of aerogel samples were measured by N_2 adsorption−desorption porosimetry (Quantachrome Nova 2200e) after degassing at 60 °C for 24 h. The specific surface area was calculated by using the multipoint BET method (five points on the adsorption curve, maximum p/p_0 = 0.30). The pore size distribution was calculated from the desorption curves by using the BJH method.

The particle size distribution of hydrated aerogel particles was measured by using a hemocytometer and image analysis after wet grinding the samples by a Potter-Elvehjem tissue grinder (10 min) and sonication (15 min). Images were taken from c = 0.5 mg mL^{-1} suspensions with a 1.3 MP USB microscope camera. The ImageJ software was used for calculating the size distribution of the particles. Additionally, the size distribution of aerogel particles was measured by laser diffraction light scattering (LDLS, MALVERN Mastersizer 2000) using conventional instrument setup and operation. Angular scattering intensity data were evaluated by the instrument controlling software. A representative refraction index of 1.006 was used in the calculations.

The zeta potential of wet ground aerogels (see the protocol above) was measured at a final aerogel concentration of c = 0.1 mg mL^{-1} on a MALVERN Zetasizer Nano ZS instrument using a conventional instrument setup and operation.

2.4. Batch Adsorption Experiments. Conventional batch adsorption experiments were performed at constant pH. A dilute HNO_3 solution of a predefined pH between 4.0 and 6.0 was prepared by using ultrafiltered water and a standardized 0.010 M HNO_3 stock solution. This dilute HNO_3 solution was used to prepare and dilute all suspensions, solutions, and other aqueous mixtures.

All solutions, suspensions, and other mixtures were prepared and stored in acid-treated (cc HNO_3) glass or Teflon vessels suitable for trace metal analysis.

Aerogel adsorbents were prepared in c = 0.40 mg mL^{-1} aqueous suspension. The dry aerogel was wet ground in dilute HNO_3 solution by using a Potter-Elvehjem tissue grinder for 10 min. The suspension was sonicated (ARGO LAB DU-32) for 15 min and then stirred for 20 min at 300 rpm on a magnetic stirrer using a 1.0 cm Teflon-coated rod. This protocol ensures the highly reproducible production of aerogel suspensions that do not settle or aggregate in the time scale of the adsorption experiments.

Metal ion stock solutions (50−250 mg L^{-1} for the metal ions) were prepared by dissolving solid metal nitrates in dilute HNO_3 solution. The pH of the stock solutions was checked and set by using the calibrated double-junction pH electrode. Metal ion containing samples were prepared for the adsorption experiments by the dilution of the metal ion stock solutions. The pH and the initial metal ion concentrations of these samples were measured prior to adding the adsorbent.

Batch adsorption experiments were performed by mixing the aerogel suspension with a metal ion solution by following a standardized protocol. The concentration of the aerogel was kept constant, and the initial concentrations of metal ions were varied in the final mixtures. Adsorption samples were always prepared by mixing 2.00 mL of metal ion solution of different concentration and 8.00 mL of aerogel suspension. The initial concentrations of metal ions in the resulting 10.0 mL samples were between 1.0 and 50 mg L^{-1}. The heterogeneous samples were agitated with a magnetic stirrer typically for 2 h to reach equilibrium. Then the samples were quantitatively transferred into plastic tubes (PP) and centrifuged for 20 min at 3500 rpm (VWR MEGASTAR 1.6 R). The supernatant was separated from the pellet, and the metal ion contents of both phases were measured by elemental analysis. All experiments were performed at least in three replicates.

Another series of independent batch adsorption measurements were conducted using the above-described protocol at initial metal ion concentrations between 30 and 950 μg L^{-1}. The rationale is that toxic heavy metal ions can realistically be present at this concentration range in natural water bodies.

Independent batch adsorption measurements were conducted by using water samples collected from a natural pond with a rich flora and fauna. The natural water was not pretreated, and its pH is 6.9. These water samples were spiked with solid $Hg(NO_3)_2$ to obtain c_0(Hg) from 0.50 to 50 mg L^{-1}. The spiked samples were stable; no precipitation of Hg(II) was detected in 4 h (*vide infra* in section 2.6). Batch adsorption measurements were conducted by using the same experimental protocol as for the above-described laboratory water (distilled water) samples.

Metal ion concentrations were determined by elemental analysis using ICP-OES. The initial concentrations of metal ions prior to adsorption (c_0) were measured directly from the sample solutions. The concentrations of the aqueous metal ions after the establishment of the adsorption equilibria were measured from the centrifugation supernatants. The absorbed amounts of metal ions were measured in the centrifugation pellets after digesting the aerogels. The applied analytical protocols are given later.

It was proved by independent experiments that the pH of a heterogeneous sample is constant during the establishment of the adsorption equilibrium in a batch adsorption experiment. The pH of the centrifugation supernatant was measured for multiple samples of various initial metal ion concentrations, and the maximum difference between the initial pH and the pH measured after centrifugation was maximum 0.21 units. Therefore, the online pH correction was not applied in any of the adsorption experiments.

The above detailed experimental layout was applied to test the performance of silica−gelatin aerogels for the adsorption of Hg(II), Cu(II), Cd(II), Co(II), Pb(II), Ni(II), Ag(I), and Zn(II) ions. A series of silica−gelatin hybrid aerogels of 4, 11, 18, and 24 wt %

DOI: 10.1021/acsanm.9b01903
ACS Appl. Nano Mater. 2020, 3, 195−206

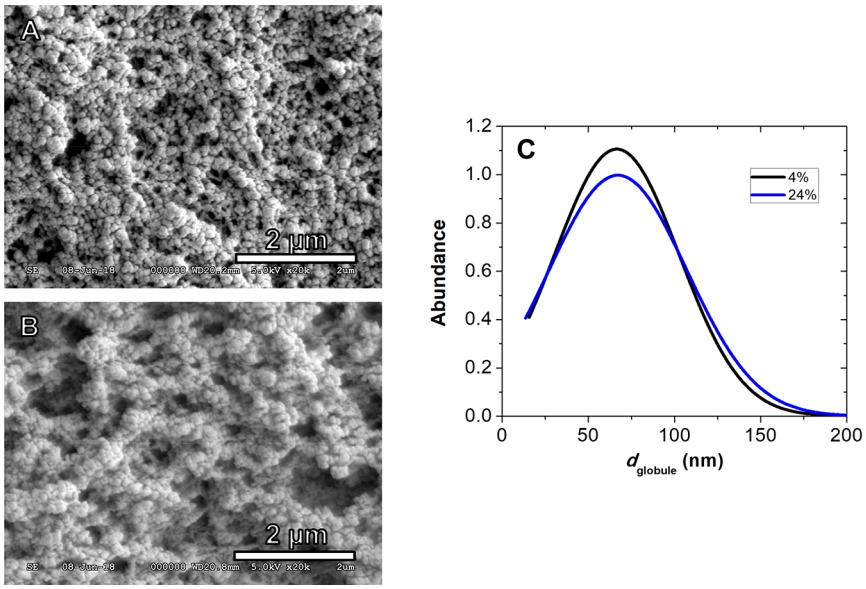

Figure 1. Scanning electron micrographs at 20K magnification of silica−gelatin hybrid aerogels of 4 wt % (A) and 24 wt % (B) gelatin content. The scale bars represent 2 μm. (C) Size distribution of the primary blocks (globules) of the silica−gelatin aerogels.

gelatin content were tested. The parent, gelatin-free silica aerogel, was used as a control.

2.5. Selectivity of Adsorbent. The adsorption of Hg(II), Cu(II), Cd(II), Co(II), Pb(II), Ni(II), Ag(I), and Zn(II) ions was studied on silica−gelatin aerogels in batch experiments, both individually and in the simultaneous presence of multiple metal ions. A series of experiments were conducted in the presence of two competing ions in the following pairs: Hg(II) + Ag(I), Hg(II) + Cd(II), Hg(II) + Cu(II), and Hg(II) + Ni(II). An additional selectivity test was performed in the simultaneous presence of six competing ions: Hg(II) + Cd(II) + Cu(II) + Zn(II) + Co(II) + Pb(II). All of these batch adsorption experiments were conducted at several different initial concentrations of metal ions in the range from 5 to 50 mg L^{-1}. All experiments were performed at least in three replicates.

2.6. Hydrolysis of Metal Ions. To ensure the reliability of the results of the adsorption experiments, it is important to study the possibility of the spontaneous hydrolysis or precipitation of the metal ions. Metal ion solutions (1−50 mg L^{-1}) were prepared in an identical way, at the same final pH, as for the adsorption experiments, but in the absence of an adsorbent. The aerogel suspension was replaced with dilute HNO_3 solution. These metal ion solutions were agitated for 2 h and centrifuged to remove any possible colloidal precipitates. Under these conditions, no concentration change was detected in any of the metal ion solutions; i.e., the recovery was 98%−102% from the centrifugation supernatants.

However, it was observed that the reproducibility of the adsorption experiments decreases in the case of Hg(II) above the initial metal ion concentration of 50 mg L^{-1} at pH = 6.0. Thus, adsorption data are reported up to c_0 = 50 mg L^{-1} for Hg(II).

2.7. Time-Resolved Adsorption Experiments. To study the rate at which the adsorption equilibrium is reached on the aerogel adsorbents, time-resolved experiments were performed at c_0 = 43 mg L^{-1} metal ion concentrations. The same protocol was used as in the case of the batch experiments (section 2.4), but the length of the contact time (i.e., agitation by magnetic stirrer) was varied. Centrifugation was 10 min. The time dependency of the adsorption process was studied by using minimum 5 min and maximum 120 min agitation. After reaching the preset contact time, the samples were removed from the magnetic stirrer and centrifuged.

2.8. Elemental Analysis of Equilibrated Aerogels. To determine the amount of metal ions adsorbed on aerogels, the adsorbent was recovered by centrifugation after the establishment of the adsorption equilibrium, chemically digested, and analyzed by ICP-OES. Two wet digestion methods were applied by using microwave-assisted sample preparation (Milestone, Ethos Up).

In the first digestion method, aerogel pellets were quantitatively rinsed into sealable PTFE vessels with the mixture of acids used for digestion. The applied reagents were 4.00 mL of 65 wt % HNO_3 and 1.00 mL of 30 wt % H_2O_2 for ca. 3.2 mg of aerogel (cf. section 2.4). The samples were microwave heated to 200 °C and digested for 20 min. The vessels were allowed to cool, and the samples were brought to a 25.0 mL final volume with Milli-Q water. This method does not dissolve silica. Residual silica was separated by centrifugation and discarded. The supernatant was analyzed.

In the second digestion method 200 μL of 38 wt % HF was also added to the aerogel pellet (additionally to the 4.00 mL of 65 wt % HNO_3 and 1.00 mL of 30 wt % H_2O_2). The primary microwave heating program was the same as in the first case. After the vessels cooled, 1.00 mL of 4.5% H_3BO_3 was added. The H_3BO_3 containing samples were resealed and microwaved again at 160 °C for 10 min. This step is important for the neutralization of excess HF. Finally, the samples were brought to a 25.0 mL final volume with Milli-Q water.

The difference between the two digestion protocols is that in the first case only the organic part of the aerogel is digested, while in the second case the total solubilization of the aerogel, including the silica part, takes place. The metal ion concentrations of the digested samples were measured by ICP-OES using the same analytical protocols as for the supernatants of the adsorption experiments.

2.9. Desorption Experiments. The reversibility of the adsorption of metal ions was tested by washing previously equilibrated aerogel pellets with different solutions. The experimental protocol of the batch adsorption experiments was applied without modification for equilibrating aerogels with metal ions (section 2.4). The supernatant of the centrifuged sample was quantitatively decanted (and analyzed for metal ion content), and 10.0 mL of washing liquid was measured onto the aerogel pellets at preset pH. The aerogel pellets were resuspended in the washing liquid and agitated for 10−60 min, which was followed by centrifugation. The supernatants were analyzed. In separate experiments, distilled water, NaCl solution (0.50 M), and EDTA solutions (0.25 and 2.5 mM) were tested as washing liquids.

2.10. Regeneration and Recycling of Adsorbent. The metal ion equilibrated aerogel pellets were regenerated by washing with 2.5 mM EDTA solution, as detailed in section 2.9. After agitating the aerogel for 30 min in EDTA solution, the system was centrifuged. The aerogel pellet was resuspended in 10.0 mL of dilute HNO_3 solution (pH = 6.0) and centrifuged again. This step was necessary to remove

DOI: 10.1021/acsanm.9b01903
ACS Appl. Nano Mater. 2020, 3, 195−206

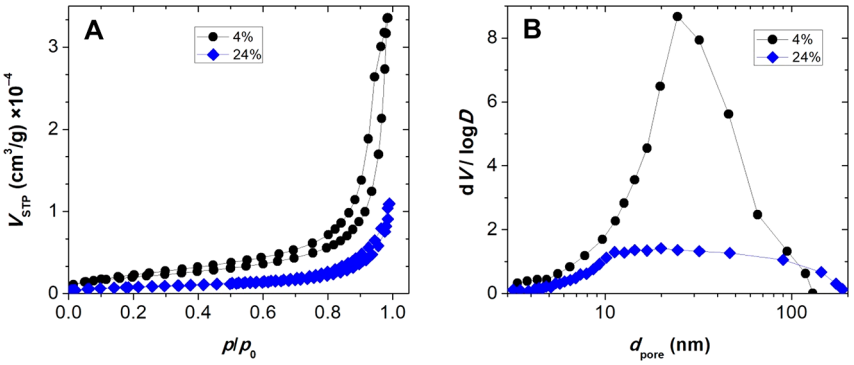

Figure 2. Nitrogen adsorption−desorption isotherms (A) and BJH pore size distribution curves (B) of silica−gelatin hybrid aerogels of 4 and 24 wt % gelatin content.

Table 1. Structural Characteristics of Silica and Silica−Gelatin Hybrid Aerogels Derived from N_2 Adsorption−Desorption Porosimetry and Light Scattering Data (cf. Figures 2 and 3 and Figure S1)

		gelatin			
	silica	4 wt %	11 wt %	18 wt %	24 wt %
S_{BET} (m^2/g)[a]	910 ± 60	800 ± 70	630 ± 60	420 ± 50	290 ± 30
V_{pore} (cm^3/g)[b]	6.2	4.9	4.5	2.3	1.7
d_{pore} (nm)[c]	32	25	32	17	20
E_{Zeta} (mV)[d] (pH = 4.0)	−20	−22	−21	−19	−14
E_{Zeta} (mV)[e] (pH = 6.0)	−30	−27	−27	−26	−23
$d_{particle}$ (μm)[f]	40	20	21	18	12

[a]BET specific surface area. [b]Total mesopore volume (BJH). [c]Mean pore diameter estimated at the maximum of the distribution curve (BJH). [d]Zeta potential measured at pH = 4.0. [e]Zeta potential measured at pH = 6.0. [f]Mean particle size estimated at the maximum of the LDLS distribution curve.

the traces of leftover EDTA from the system. The supernatant was discarded, and the regenerated aerogel was resuspended in 8.00 mL of dilute HNO_3 solution (pH = 6.0). This aerogel suspension was tested as an adsorbent for Hg(II) in batch experiments by following the standardized protocol given in section 2.4. After equilibration with Hg(II), the aerogel was regenerated again by following the above steps and reintroduced into a new cycle of batch adsorption. Altogether, five adsorption−regeneration cycles were performed with an individual sample of aerogel.

2.11. Elemental Analysis by ICP-OES. The metal contents of solutions (supernatants, washing liquids) and digested aerogel pellets were measured by inductively coupled plasma optical emission spectrometry (Agilent Technologies, ICP-OES SVDV 5100) using always the same protocol. Solution samples were acidified with one drop of cc HNO_3 immediately after preparation and were measured no longer than 2 h in storage. Five-point calibration was applied (0−50 mg L^{-1}), diluted from monoelement standard solutions of 1000 mg L^{-1} (Scharlau). Intensity values were collected at three different wavelengths of each metal. Metal concentrations were calculated by using the optical lines that gave the best signal-to-background ratio for each metal.

The concentrations of at least three independent parallel samples were averaged. The relative standard deviation (RSD) was calculated. The ICP-OES experimental parameters are given in Table S1 of the Supporting Information.

3. RESULTS AND DISCUSSION

3.1. Aerogel Characterization. *3.1.1. Scanning Electron Microscopy (SEM).* Representative SEM images (20K magnification) of silica−gelatin hybrid aerogels of 4 and 24 wt % gelatin content are shown in Figure 1. The hybrid aerogel backbones are built from spherical blocks (globules), which is a general characteristic of silica-based aerogels. The size of these blocks is in the range of $d_{globule}$ = 40−100 nm, and it is independent from the gelatin content of the hybrids: $d_{4wt\%}$ = 66 ± 36 nm and $d_{24wt\%}$ = 68 ± 40 nm (cf. Figure 1C). Although the fundamental morphology of the silica−gelatin aerogels is similar to that of pure silica aerogels, both the number and size of macropores increase systematically with the increasing gelatin content of the hybrids.

3.1.2. N_2 Adsorption−Desorption Porosimetry. The nitrogen adsorption−desorption isotherms of the dry silica and silica−gelatin aerogels are type IV (H3) hysteresis curves according to the IUPAC classification (Figure 2A). This is characteristic for mesoporous materials with some macropores. Pore size distribution curves are calculated by the BJH method from the desorption isotherms. This evaluation also shows the dual mesoporous and macroporous characteristics of the hybrids (Figure 2B). Further structural parameters of the aerogels are listed in Table 1. The BET specific surface area (S_{BET}), the total mesopore volume (V_{pore}), and the mean pore diameter (d_{pore}) decrease systematically with the increasing gelatin content of the hybrids.

The SEM pictures in Figure 1 evidently show that the apparent decrease of the S_{BET} and V_{pore} structural parameters in Table 1 at high gelatin content is not due to the loss of porosity but due to the formation of macropores. As a consequence of the working principle of N_2 porosimetry, macropores are excluded from the analysis. Notably, the total porosity of the aerogel is still high even at 24 wt % gelatin content.

3.1.3. Particle Size of Hydrated Aerogels. The particle size distribution of silica and silica−gelatin aerogels was measured by following the wet grinding of the samples using a standardized protocol (cf. section 2.3). Both the position of the maximum and the width of the particle size distribution

DOI: 10.1021/acsanm.9b01903
ACS Appl. Nano Mater. 2020, 3, 195−206

curve decrease systematically with the increasing gelatin content of the hybrid aerogels (Figure 3 and Table 1).

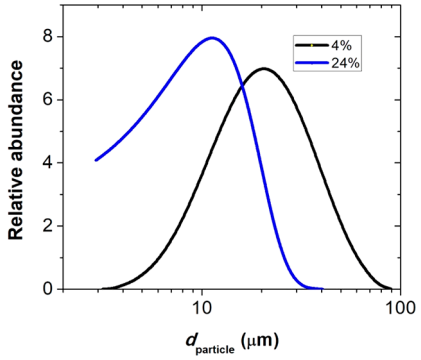

Figure 3. Particle size distribution of hybrid aerogel particles of 4 and 24 wt % gelatin measured by laser diffraction light scattering.

3.1.4. Zeta Potential of Aerogel Particles. The zeta potential (E_Z) of hybrid aerogel particles was studied in the pH range from 3.0 to 7.4. Data are summarized in Table 1 and Figure S1. The zeta potential of the hybrid aerogels systematically increases with increasing gelatin content, regardless of the pH. The isoelectric point of silica is at ca. pH = 3.5, and that of aqueous type A gelatin is at ca. pH = 5.5, which gives a natural explanation for the increase of E_Z with gelatin content.[58]

3.2. Adsorption Experiments. *3.2.1. Selectivity of Silica–Gelatin Aerogels.* Silica–gelatin aerogels of 4–24 wt % gelatin content were tested to adsorb aqueous Hg(II) Cu(II), Cd(II), Co(II), Pb(II), Ni(II), Ag(I), and Zn(II) in batch adsorption experiments. The adsorption of metal ions was studied individually and also in the simultaneous presence of multiple metal ions. The operating pH was either pH = 4.0 or pH = 6.0. All of the batch adsorption experiments (as detailed in sections 2.4 and 2.5) consistently show that silica–gelatin hybrid aerogels have unprecedentedly high selectivity for binding Hg(II). The amounts of metal ions adsorbed by the 24 wt % hybrid aerogel at pH = 6.0 at c_0 = 10 mg L^{-1} initial metal ion concentration are shown in Figure 4A. This figure was constructed by using the compiled results of the experiments where multiple competing metal ions were present in the same solution (cf. section 2.5). The only ion which binds to the hybrid aerogels besides Hg(II) is Ag(I), but competitive adsorption tests confirmed the superior selectivity of the adsorbents toward Hg(II) (Figure 4B). With the exception of these two ions, none of the metal ions showed significant affinity to bind to the hybrid aerogels in the studied pH range.

3.2.2. Optimal Conditions for Adsorption of Hg(II). To evaluate the adsorption characteristics of the hybrid aerogels toward Hg(II), the effects of pH, the gelatin content of the adsorbent, and the initial aqueous Hg(II) concentration were tested.

In general, high pH facilitates the adsorption of metal cations on negatively charged adsorbents, but high pH can also cause the hydrolysis of the metal cations. Thus, the optimum pH for adsorption is where the surface of the adsorbent is already negatively charged, and the metal ions still do not hydrolyze. The isoelectric point of the hybrid aerogels is around pH = 4.0, and Hg(II) hydrolyses above pH = 6.0, even at low concentrations. (These considerations are discussed further in section 3.5.) As expected, the best adsorption capacity was measured at the highest applicable pH value, at pH = 6.0. A significantly lower adsorption capacity was obtained at pH = 4.0, as seen in Figure S2.

Isotherms measured at pH = 6.0 for the adsorption of aqueous Hg(II) on aerogels of different gelatin contents are shown in Figure 5. These isotherms are far from saturation at c_0 = 43 mg L^{-1} initial Hg(II) concentration, but higher concentrations were not applied to avoid the complications arising from the hydrolysis of Hg(II). Evidently, the 24 wt % hybrid aerogel binds the largest amount of Hg(II), that is, q_E = 78.3 ± 3.8 mg g^{-1} at c_0 = 43 mg L^{-1}. The adsorption capacity of the hybrid aerogels markedly increases with increasing gelatin content, indicating that the biopolymer constituent is the main binder of Hg(II). However, the adsorption characteristics of the hybrid aerogels show a complex dependence on their gelatin content, which is further discussed in section 3.5.

The data points of the batch adsorption experiments in Figure 5 can be adequately fitted with both the Langmuir (eq 1) and the Freundlich (eq 2) sorption isotherm models:[59]

$$q_E = \frac{[Hg(II)]_{ads}}{c_{aerogel}} = \frac{K_L[Hg(II)]_{sol}S}{1 + K_L[Hg(II)]_{sol}} \quad (1)$$

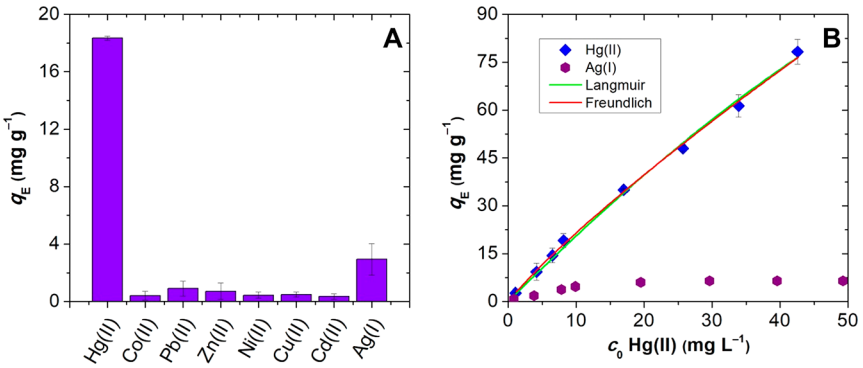

Figure 4. (A) Amounts of metal ions adsorbed at equilibrium by the 24 wt % hybrid aerogel at pH = 6.0, c_0 = 10 mg L^{-1} metal ion, and 0.32 mg mL^{-1} aerogel (measured in the simultaneous presence of competing metal ions). The diagram shows the compiled results of all the metal ion competition experiments described in section 2.5. (B) Symbols: experimental isotherms describing the simultaneous adsorption of Hg(II) and Ag(I) on the 24 wt % hybrid aerogel at pH = 6.0, 0.32 mg mL^{-1} aerogel. Lines: nonlinear fits using different isotherm models.

DOI: 10.1021/acsanm.9b01903
ACS Appl. Nano Mater. 2020, 3, 195–206

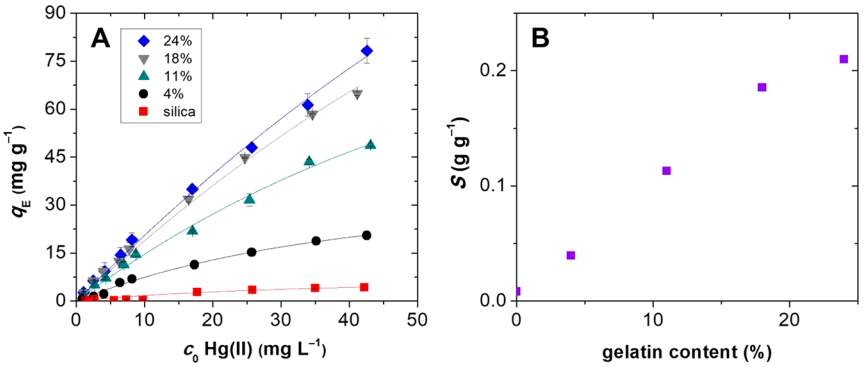

Figure 5. (A) Adsorption isotherms of Hg(II) on silica and silica−gelatin hybrid aerogels at pH = 6.0 and 0.32 mg mL^{-1} aerogel concentration. Symbols: experimental points. Lines: nonlinear fits using the Langmuir isotherm model. (B) Change of the adsorption capacity of the aerogels with their gelatin content estimated by fitting with the Langmuir model.

$$q_E = \frac{[Hg(II)]_{ads}}{c_{aerogel}} = K_F([Hg(II)]_{sol})^n \quad (2)$$

Here, q_E is the amount of metal ions adsorbed in equilibrium per unit weight of adsorbent (mg g^{-1}), $[Hg(II)]_{ads}$ is the solution-equivalent concentration of adsorbed Hg(II) at equilibrium (mg L^{-1}), $c_{aerogel}$ is the concentration of the aerogel (g L^{-1}), $[Hg(II)]_{sol}$ is the equilibrium concentration of aqueous Hg(II) (mg L^{-1}), S is the adsorptive capacity of the adsorbent (mg g^{-1}), K_L is the Langmuir equilibrium constant (L mg^{-1}), K_F is the Freundlich equilibrium constant (mg g^{-1}), and n is the empirical adsorption intensity of the Freundlich model.

Isotherm fitting was performed nonlinearly by using the Levenberg−Marquardt least-squares algorithm. Representative results are shown in Figure 5 and Figure S3, and the estimated parameters are given in Table S2. The goodness-of-fit levels are excellent in the cases of both the Langmuir and the Freundlich isotherm models, which is clearly expressed by the low ±SD values associated with the nonliner regression processes (cf. Table S2). Because of the low curvature of the experimental isotherms, the goodness-of-fit was practically equivalent for the Langmuir and the Freundlich models. Fortunately, the two models are in consensus regarding the increasing adsorption capacity of the aerogels with increasing gelatin content because both parameter S (Langmuir) and parameter K_F (Freundlich) increase systematically with increasing gelatin content (Figures S3C,D).

A maximum adsorption capacity of 209 ± 60 mg g^{-1} can be extrapolated for the 24 wt % gelatin hybrid by using the Langmuir model, complemented with an equilibrium constant of K_L = 0.032 ± 0.013 L mg^{-1} (cf. Table S2). However, the maximum adsorption capacity could not be reached in the applied experimental setup because the equilibrium constant K_L is too low for the saturation of the active sites at c_0 = 43 mg L^{-1} aqueous Hg(II) concentration.

3.2.3. Time-Resolved Adsorption Experiments. Time-resolved adsorption experiments were performed under the same conditions as the batch adsorption tests. As seen in Figure 6, the adsorption equilibrium is already established after 5 min of agitation (and 10 min of centrifugation) even at the highest c_0 = 43 mg L^{-1} initial Hg(II) concentration. The rate of the binding of Hg(II) is practically independent of the initial Hg(II) concentration and the gelatin content of the aerogel (Figure 6). The extremely fast establishment of the adsorption equilibrium is a major advantage regarding the functionality of the silica−gelatin aerogel adsorbents.

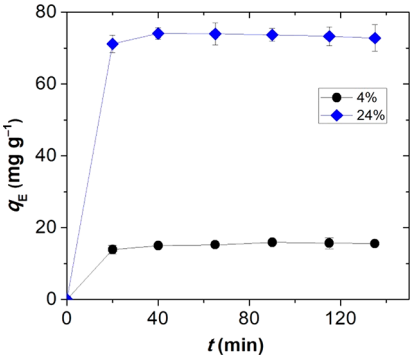

Figure 6. Rate of adsorption of Hg(II) on silica−gelatin hybrid aerogels of 4 and 24 wt % gelatin content. The x-axis of the figure shows the total contact time, which is the sum of the agitation time and the centrifugation time. pH = 6.0; c_0 = 43 mg L^{-1} Hg(II), 0.32 mg mL^{-1} aerogel concentration.

3.2.4. Analysis of Hg(II) Equilibrated Aerogels. The aerogels equilibrated with aqueous Hg(II) in batch experiments were recovered by centrifugation. The wet pellets were digested under different conditions to investigate the localization of the adsorbed Hg(II) in the silica and the gelatin constituents of the hybrid aerogel backbone.

First, the gelatin part was selectively digested by using HNO_3 and H_2O_2 (section 2.8). The undissolved silica component was discarded, and the remaining solution was analyzed. The main portion (85−90%) of adsorbed Hg(II) was recovered by this method (Table 2). Another digestion experiment was performed by using HNO_3, H_2O_2, and HF

Table 2. Partitioning of Hg(II) in Equilibrium between the Aqueous Phase and the Silica−Gelatin Hybrid Aerogel Adsorbent of 24 wt % Gelatin[a]

c_0(Hg(II)) (mg L^{-1})	Hg(II) in supernatant (%)	Hg(II) bound to the gelatin component of the aerogel (recovered by HNO_3, H_2O_2) (%)	Hg(II) bound to the silica component of the aerogel (recovered by additional HF) (%)
10	40.3	54.8	4.9
43	40.5	49.9	9.6

[a]Based on the result of digestion experiments, the overall recovery of the initial amount of Hg(II) is 96−104%. pH = 6.0, 0.32 mg mL^{-1} aerogel concentration.

DOI: 10.1021/acsanm.9b01903
ACS Appl. Nano Mater. 2020, 3, 195−206

(section 2.8). This protocol ensured the complete solubilization of the aerogel pellets, and the results confirmed the complete (96−104%) recovery of adsorbed Hg(II) (Table 2).

The partitioning of Hg(II) in an equilibrium system at different initial concentrations is given in Table 2. The results in Table 2 can be interpreted by assuming that the portion of Hg(II) that can be recovered exclusively by the total solubilization of the adsorbent with HF is strongly bound to the silica constituent of the hybrid aerogel and the part of Hg(II) that can be recovered by partial solubilization is bound primarily to gelatin. This analysis highlights that Hg(II) has a high preference toward the gelatin part of the hybrid silica−gelatin aerogels. The lower affinity of Hg(II) toward pure silica is also confirmed by the batch adsorption experiments performed with the parent silica aerogel (cf. Figure 5).

3.2.5. Adsorption of Hg(II) at Realistic Conditions. The concentration of dissolved Hg(II) in natural water bodies is most often below 1.0 mg L^{-1}. Therefore, independent batch adsorption experiments were conducted by using initial Hg(II) concentrations between 0.030 and 1.0 mg L^{-1} at pH = 6.0. The removal efficiency of aqueous Hg(II) is between 93% and 91% in this concentration range by using 0.32 g L^{-1} of the 24 wt % gelatin aerogel. The corresponding adsorption isotherm is given in Figure 7.

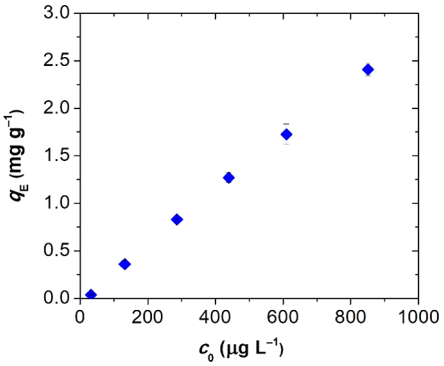

Figure 7. Adsorption isotherm of Hg(II) on 24 wt % silica−gelatin hybrid aerogel at pH = 6.0 and 0.32 mg mL^{-1} aerogel concentration. The initial concentration of Hg(II) is below 1.0 mg L^{-1} in each experiment, and Hg(II) removal is between 91% and 93%.

Several organic and inorganic compounds are present in natural waters that fundamentally effect the chemical speciation of aqueous mercury ions. These are mainly redox-active compounds (e.g., sulfites and nitrites) or complex forming compounds (e.g., chelating ligands). Because of altering the speciation of aqueous mercury ions, the presence of these compounds can radically change the removal efficiency of Hg(II) by adsorption (*vide infra* section 3.5.2). The performance of the hybrid aerogel of 24 wt % gelatin content was tested in such a natural environment. Water was collected from a natural pond with a rich flora and fauna and spiked with solid $Hg(NO_3)_2$. Batch adsorption measurements were conducted by using the same experimental protocol as in the case of the tests with distilled water. As seen in Figure 8, the Hg(II) removal efficiency of the hybrid aerogel is not compromised in the tested natural water sample.

3.3. Desorption of Hg(II). Aerogel pellets equilibrated with Hg(II) in batch adsorption experiments were washed with different solutions to examine the reversibility of the binding of Hg(II) (section 2.9). The desorption of Hg(II) is negligible

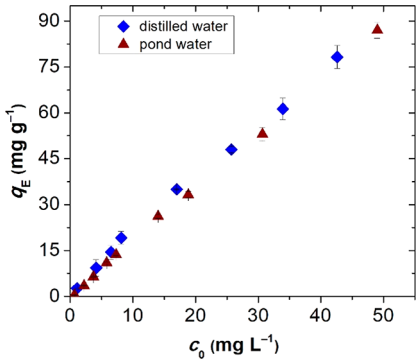

Figure 8. Adsorption isotherms of Hg(II) on 24 wt % silica−gelatin hybrid aerogel recorded in pure water (distilled water) and in a water sample obtained from a natural pond with rich flora and fauna (0.32 mg mL^{-1} aerogel concentration).

(maximum 10%) when the pellet is washed with water. Approximately 62% of the adsorbed Hg(II) is recovered by using 0.50 M NaCl solution, and recovery is increased to ca. 91% by using 0.25 mM EDTA solution. Complete recovery (95−102%) was achieved by washing the pellet with 2.5 mM EDTA solution. These results also demonstrate that the binding of Hg(II) is reversible. Because common complexing agents can induce the nearly quantitative desorption of Hg(II), it means that the metal ions are not reduced to elementary Hg on the aerogel surface.

It was proved in independent time-resolved experiments that the rate of the desorption process is similarly rapid as the adsorption process. The desorption equilibrium is established in 10 min contact time. This finding is in line with the high kinetic lability of Hg(II) in complex formation reactions.[60]

3.4. Regeneration and Recycling of Aerogel Adsorbent. After equilibrating the aerogel adsorbents with aqueous Hg(II), the adsorbent can be effectively recovered by centrifugation and regenerated by washing with 2.5 mM EDTA solution (cf. section 2.10). The regenerated silica−gelatin aerogel of 24 wt % gelatin content shows only a minor decrease (maximum 9% compared to the first cycle) in adsorption capacity even after five cycles of adsorption and regeneration, as shown in Figure 9. This highlights that practical utilization of the presented hybrid aerogel adsorbents is feasible.

3.5. Mechanism of Adsorption of Hg(II) on Silica−Gelatin Aerogel. *3.5.1. Effect of Aerogel Composition and Structure.* Several factors have an effect on the kinetic and thermodynamic properties of the adsorption of Hg(II) on silica−gelatin aerogels. The most important factors that control these properties are the number of active sites on the hybrid adsorbent, its particle size, porosity, and zeta potential at the pH of the aqueous phase.

Gelatin provides the active sites for Hg(II) binding; thus naturally, a higher gelatin content results in higher adsorption capacity for the aerogels (cf. Figure 5 and Table S2). The adsorption capacity also depends on the size distribution of the adsorbent dispersed in the aqueous media, as smaller particles lead to higher overall surface area. As a positive effect, aerogels of high gelatin content yield smaller particles when hydrated (cf. Figure 3 and Table 1). This is explained by taking into account that the collagen molecules of the backbone are held together by secondary chemical forces that are easily disrupted

DOI: 10.1021/acsanm.9b01903
ACS Appl. Nano Mater. 2020, 3, 195−206

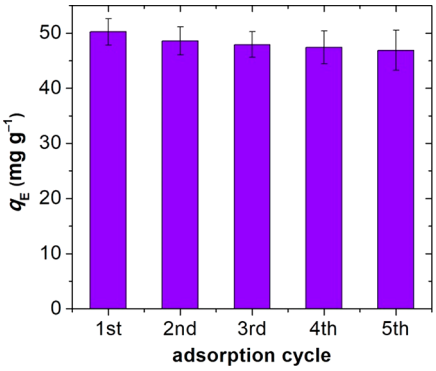

Figure 9. Recycling the silica−gelatin aerogel adsorbent of 24 wt % gelatin content. After equilibrating with aqueous Hg(II), the aerogel was recovered, regenerated by washing with 2.5 mM EDTA solution, and reintroduced into a new batch adsorption cycle. The adsorbed amount of Hg(II) in each cycle is given in the plot. pH = 6.0; c_0 = 30 mg L^{-1} Hg(II), 0.32 mg mL^{-1} aerogel concentration.

by hydration, whereas the hydrolysis of the covalent silica network is limited.

The zeta potential of the hybrid aerogels increases with their increasing gelatin content. Under pH = 3.5, the surfaces of the hybrid aerogels lose their negative charges, which reduces their ability to bind cations. In the case of the highest gelatin content (24 wt %), the surface of the hybrid aerogel is still negatively charged in the experimentally useful pH range.

Unfortunately, a detrimental side effect arises when the gelatin content of the hybrid aerogel is high. That is gelatin induces the swelling of the hydrated particles and the distortion of the pore structure. The extensive swelling of the high-gelatin hybrid backbone results in the partial collapse of the open porous structure and the decrease of the specific surface area. Thus, the increase of the number of the active sites with increasing gelatin content can be counterbalanced by the collapse of the aerogel pores. Owing to this effect, the adsorption capacity of the hybrid aerogels cannot be elevated above a threshold value by increasing the gelatin content of the adsorbent, and adsorption capacity is not proportional anymore with gelatin content at high (18−24 wt %) gelatin contents (cf. Figure 5, Figure S3, and Table S2). (According to our experience, there is an elevated risk for the formation of local inhomogeneities in the aerogel backbone during the synthetic procedure above 24 wt % gelatin content; thus, hybrids of higher gelatin content were not prepared.)

An important addition to this mechanistic explanation is that the silica constituent of the hybrid aerogels effectively preserves the porosity of the adsorbent to a certain extent and prevents the total collapse of the pore network in water. This enables the fast transport of aqueous ions throughout the particles, which in turn ensures the fast establishing of the adsorption equilibrium and the conservation of the adsorption capacity.

3.5.2. Speciation of Aqueous Hg(II) and Selectivity of Silica−Gelatin. Hydrated mercury(II) ions form a variety of coordination compounds with ligands commonly found in aqueous solutions and natural waters. The two simplest and most abundant ligands that form high-stability complexes with Hg(II) are the inorganic anions OH^- and Cl^-.[61] The formation of hydroxo−Hg(II) complexes, i.e., the hydrolysis of aqueous Hg(II), starts at around pH = 2.0 and becomes complete at around pH = 7.0 with the formation of the charge-neutral $Hg(OH)_2$. Below pH = 7.0 aqueous Hg(II) is mostly found in cationic forms (Hg^{2+} and $HgOH^+$), in the absence of other ligands. In the presence of Cl^-, the mixed-ligand complex HgClOH forms, starting at around pH = 4.0. Therefore, high pH and high Cl^- concentration significantly decrease the relative concentration of positively charged aqueous Hg(II) species.[61,62] Evidently, other natural ligands, e.g., humic acids, also give more or less stable complexes with aqueous Hg(II).[40]

When aqueous Hg(II) species react with a solid adsorbent, a stable interaction can form between the adsorbent and Hg(II) only in such cases when the coordination of the functional groups of the adsorbent to Hg(II) is stronger than the coordination of OH^- and Cl^- (and other natural ligands) to Hg(II) in the original solution. In other words, efficient Hg(II) removal, i.e., high performance adsorption, can be achieved only in such cases when there is a strong and preferably specific chemical interaction between Hg(II) and the functional groups of the adsorbent. The adsorbent is in competition with the original ligands (e.g., OH^- and Cl^-) of Hg(II) for complexing and binding the metal ion.

In this study we proved that even in a natural water sample, the 24 wt % gelatin containing silica−gelatin aerogel efficiently adsorbs aqueous Hg(II) (cf. section 3.2.5 and Figure 8). This implies that there are strong coordination bonds between the side chains of the protein constituents of the hybrid aerogel and Hg(II) that can repulse other ligands (e.g., OH^-, Cl^-, and natural compounds) from the coordination sphere of Hg(II). The coordination bonds between gelatin in the aerogel and Hg(II) can be disrupted only by the addition of an even stronger ligand, the chelate forming EDTA (cf. sections 3.3 and 3.4). This fact also proves that no redox reaction takes place between the aerogel and Hg(II), as the formation of zerovalent Hg would render the adsorption irreversible. Furthermore, the generally high kinetic lability of the Hg(II) complexes accounts for the fast adsorption and desorption steps.

The high affinity of gelatin and collagen proteins toward Ag(I) and Hg(II) are well-known since the dawn of photography.[63,64] This effect can be attributed to the high number of $-NH_2$ and, more importantly, −SH and −S−S− functional groups in the protein side chains. These functional groups are soft Lewis bases that are ideal ligands for soft metal ions, such as Hg(II) and Ag(I) (Lewis acids). To form stable complexes with metal ions of harder character (e.g., Pb^{2+}, Cd^{2+}, Cu^{2+}, and Zn^{2+}), the presence of $-NH_2$, −OH, and −COOH functional groups would be needed on the adsorbent. Thus, the abundance of soft functional groups together with the near absence of hard functional groups in gelatin side chains accounts for the selectivity of silica−gelatin aerogels toward binding Hg(II).

4. CONCLUSIONS

Supercritically dried, mesoporous silica−gelatin hybrid aerogels of 4−24 wt % gelatin content are excellent adsorbents for aqueous Hg(II). These hybrids show exceptionally high selectivity toward Hg(II) even in the simultaneous presence of multiple types of competing aqueous metal ions. The best adsorption capacity was measured at pH = 6.0 by using the aerogel of 24 wt % gelatin content. The experimental isotherms can be fitted with both the Langmuir and the Freundlich models with practically the same goodness-of-fit results. Extrapolating the Langmuir isotherm shows a maximum adsorption capacity for the 24 wt % gelatin hybrid aerogel of

DOI: 10.1021/acsanm.9b01903
ACS Appl. Nano Mater. 2020, 3, 195−206

S = 209 mg g^{-1} for Hg(II) with an equilibrium constant of K_L = 0.032 L mg^{-1}. Time-resolved experiments demonstrate that the adsorption equilibrium is established extremely fast, in 15 min of contact time. The quantitative desorption of Hg(II) can be achieved by washing the equilibrated aerogel with 2.5 mM EDTA solution for 10 min. This fact also indicates that Hg(II) is reversibly bound to the aerogel surface, most probably by selective coordination bonds to protein side chains.

The gelatin content of the hybrid−silica gelatin aerogels has a complex effect on their structural characteristics and consequently on their adsorption properties. Increasing the gelatin content of the aerogel increases the number of active sites and decreases the particle size of the degraded aerogel in water. These effects are advantageous for adsorption processes. In contrast, high gelatin content results in the swelling of the aerogel particles and the partial collapse of the open porous structure. Because of these counteracting effects, the adsorption capacity of the hybrid aerogels does not increase proportionally with the gelatin content at large gelatin contents.

Based on the previously discussed results, the silica−gelatin hybrid aerogel of 24 wt % gelatin can be regarded as a high performance and highly selective Hg(II) adsorbent. The maximum adsorption capacity of this hybrid is ca. 200 mg g^{-1}, which translates to 91% Hg(II) removal at 1.0 mg L^{-1} initial Hg(II) concentration at an adsorbent concentration of 0.32 g L^{-1}. Thus, the adsorption capacity of the 24 wt % silica−gelatin aerogel is approximately the same as that of functionalized graphene adsorbents (e.g., cysteamine-functionalized graphene oxide, graphene diatom silica aerogel, graphene decorated with αFeOOH, etc.) reported recently.[9,16,27,28,40,44,65] (A comprehensive table is given in ref 27.) The main drawback of the hybrid aerogel is that a higher concentration is needed from this adsorbent to achieve practically complete Hg(II) removal at c_0(Hg) > 1.0 mg L^{-1}. This is rationalized by the lower Langmuir equilibrium constant (K_L = 0.032 L mg^{-1}). However, the 24 wt % hybrid aerogel establishes the adsorption equilibrium in 15 min, which is faster than for the above-described adsorbents, and practically no adsorption capacity is lost in five cycles of adsorption and regeneration. Thus, its selectivity, the fast rate of equilibration, and the option of adding further functionalities to the silica−gelatin backbone make this simple hybrid aerogel a versatile functional material.

■ ASSOCIATED CONTENT

Supporting Information

The Supporting Information is available free of charge at https://pubs.acs.org/doi/10.1021/acsanm.9b01903.

Additional experimental details, Figures S1−S3, and Tables S1 and S2 (PDF)

■ AUTHOR INFORMATION

Corresponding Author

*E-mail: kalmar.jozsef@science.unideb.hu.

ORCID

István Fábián: 0000-0002-4467-2912

József Kalmár: 0000-0002-2422-6106

Notes

The authors declare no competing financial interest.

■ ACKNOWLEDGMENTS

We are grateful to Péter Veres for the preparation of silica−gelatin hybrid aerogels and Réka Szabó and László Bazsó (University of Debrecen) for the technical assistance. Petra Herman was supported by the ÚNKP-19-3-I New National Excellence Program of the Ministry for Innovation and Technology. J.K. is grateful for the János Bolyai Research Scholarship of the Hungarian Academy of Sciences and for the New National Excellence Program (ÚNKP-19-4) of the Ministry of Innovation and Technology of Hungary for financial support. The research has been financially supported by the National Research, Development and Innovation Office, Hungarian Science Foundation (OTKA: FK_17-124571 and OTKA: K_17-124983). The research was supported by the EU and cofinanced by the European Regional Development Fund under the GINOP-2.3.2-15-2016-00008 project. Novo-Lab Ltd. (Agilent Technologies and Milestone) is acknowledged for providing the ICP-OES and Ethos Up instruments.

■ REFERENCES

(1) Vardhan, K. H.; Kumar, P. S.; Panda, R. C. A Review on Heavy Metal Pollution, Toxicity and Remedial Measures: Current Trends and Future Perspectives. *J. Mol. Liq.* **2019**, *290*, 111197.

(2) Vareda, J. P.; Valente, A. J. M.; Durães, L. Assessment of Heavy Metal Pollution from Anthropogenic Activities and Remediation Strategies: A Review. *J. Environ. Manage.* **2019**, *246*, 101−118.

(3) Joseph, L.; Jun, B.-M.; Flora, J. R. V.; Park, C. M.; Yoon, Y. Removal of Heavy Metals from Water Sources in the Developing World Using Low-Cost Materials: A Review. *Chemosphere* **2019**, *229*, 142−159.

(4) Huang, Y.; Wu, D.; Wang, X.; Huang, W.; Lawless, D.; Feng, X. Removal of Heavy Metals from Water Using Polyvinylamine by Polymer-Enhanced Ultrafiltration and Flocculation. *Sep. Purif. Technol.* **2016**, *158*, 124−136.

(5) Efome, J. E.; Rana, D.; Matsuura, T.; Lan, C. Q. Effects of Operating Parameters and Coexisting Ions on the Efficiency of Heavy Metal Ions Removal by Nano-Fibrous Metal-Organic Framework Membrane Filtration Process. *Sci. Total Environ.* **2019**, *674*, 355−362.

(6) Hosseini, S. M.; Alibakhshi, H.; Jashni, E.; Parvizian, F.; Shen, J. N.; Taheri, M.; Ebrahimi, M.; Rafiei, N. A Novel Layer-by-Layer Heterogeneous Cation Exchange Membrane for Heavy Metal Ions Removal from Water. *J. Hazard. Mater.* **2020**, *381*, 120884.

(7) Aschermann, G.; Schröder, C.; Zietzschmann, F.; Jekel, M. Organic Micropollutant Desorption in Various Water Matrices - Activated Carbon Pore Characteristics Determine the Reversibility of Adsorption. *Chemosphere* **2019**, *237*, 124415.

(8) Pyrzynska, K. Removal of Cadmium from Wastewaters with Low-Cost Adsorbents. *J. Environ. Chem. Eng.* **2019**, *7* (1), 102795.

(9) Brown, J.; Mercier, L.; Pinnavaia, T. J. Selective Adsorption of Hg 2+ by Thiol-Functionalized Nanoporous Silica. *Chem. Commun.* **1999**, *0* (1), 69−70.

(10) Chen, J.; Qu, R.; Zhang, Y.; Sun, C.; Wang, C.; Ji, C.; Yin, P.; Chen, H.; Niu, Y. Preparation of Silica Gel Supported Amidoxime Adsorbents for Selective Adsorption of Hg(II) from Aqueous Solution. *Chem. Eng. J.* **2012**, *209*, 235−244.

(11) Faghihian, H.; Nourmoradi, H.; Shokouhi, M. Removal of Copper (II) and Nickel (II) from Aqueous Media Using Silica Aerogel Modified with Amino Propyl Triethoxysilane as an Adsorbent: Equilibrium, Kinetic, and Isotherms Study. *Desalin. Water Treat.* **2014**, *52* (1−3), 305−313.

(12) Song, X.; Niu, Y.; Qiu, Z.; Zhang, Z.; Zhou, Y.; Zhao, J.; Chen, H. Adsorption of Hg(II) and Ag(I) from Fuel Ethanol by Silica Gel Supported Sulfur-Containing PAMAM Dendrimers: Kinetics, Equilibrium and Thermodynamics. *Fuel* **2017**, *206*, 80−88.

(13) Fu, Y.; Jiang, J.; Chen, Z.; Ying, S.; Wang, J.; Hu, J. Rapid and Selective Removal of Hg(II) Ions and High Catalytic Performance of the Spent Adsorbent Based on Functionalized Mesoporous Silica/

DOI: 10.1021/acsanm.9b01903
ACS Appl. Nano Mater. 2020, 3, 195−206

poly(m-Aminothiophenol) Nanocomposite. *J. Mol. Liq.* **2019**, *286*, 110746.
(14) Pérez-Quintanilla, D.; del Hierro, I.; Fajardo, M.; Sierra, I. Mesoporous Silica Functionalized with 2-Mercaptopyridine: Synthesis, Characterization and Employment for Hg(II) Adsorption. *Microporous Mesoporous Mater.* **2006**, *89* (1), 58−68.
(15) Sun, J.; Chen, Z.; Ge, M.; Xu, L.; Zhai, M. Selective Adsorption of Hg(II) by γ-Radiation Synthesized Silica-Graft-Vinyl Imidazole Adsorbent. *J. Hazard. Mater.* **2013**, *244*−*245*, 94−101.
(16) Štandeker, S.; Veronovski, A.; Novak, Z.; Knez, Ž. Silica Aerogels Modified with Mercapto Functional Groups Used for Cu(II) and Hg(II) Removal from Aqueous Solutions. *Desalination* **2011**, *269* (1), 223−230.
(17) Ma, F.; Qu, R.; Sun, C.; Wang, C.; Ji, C.; Zhang, Y.; Yin, P. Adsorption Behaviors of Hg(II) on Chitosan Functionalized by Amino-Terminated Hyperbranched Polyamidoamine Polymers. *J. Hazard. Mater.* **2009**, *172* (2−3), 792−801.
(18) Zhou, L.; Liu, Z.; Liu, J.; Huang, Q. Adsorption of Hg(II) from Aqueous Solution by Ethylenediamine-Modified Magnetic Cross-linking Chitosan Microspheres. *Desalination* **2010**, *258* (1), 41−47.
(19) Monier, M.; Abdel-Latif, D. A. Preparation of Cross-Linked Magnetic Chitosan-Phenylthiourea Resin for Adsorption of Hg(II), Cd(II) and Zn(II) Ions from Aqueous Solutions. *J. Hazard. Mater.* **2012**, *209*−*210*, 240−249.
(20) Zhang, D.; Wang, L.; Zeng, H.; Yan, P.; Nie, J.; Sharma, V. K.; Wang, C. A Three-Dimensional Macroporous Network Structured Chitosan/cellulose Biocomposite Sponge for Rapid and Selective Removal of mercury(II) Ions from Aqueous Solution. *Chem. Eng. J.* **2019**, *363*, 192−202.
(21) Zeng, H.; Wang, L.; Zhang, D.; Wang, F.; Sharma, V. K.; Wang, C. Amido-Functionalized Carboxymethyl Chitosan/montmorillonite Composite for Highly Efficient and Cost-Effective Mercury Removal from Aqueous Solution. *J. Colloid Interface Sci.* **2019**, *554*, 479−487.
(22) Chauhan, K.; Singh, P.; Singhal, R. K. New Chitosan−Thiomer: An Efficient Colorimetric Sensor and Effective Sorbent for Mercury at Ultralow Concentration. *ACS Appl. Mater. Interfaces* **2015**, *7* (47), 26069−26078.
(23) Chandra, V.; Kim, K. S. Highly Selective Adsorption of Hg2+ by a Polypyrrole−reduced Graphene Oxide Composite. *Chem. Commun.* **2011**, *47* (13), 3942−3944.
(24) Ma, Y.-X.; Xing, D.; Shao, W.-J.; Du, X.-Y.; La, P.-Q. Preparation of Polyamidoamine Dendrimers Functionalized Magnetic Graphene Oxide for the Adsorption of Hg(II) in Aqueous Solution. *J. Colloid Interface Sci.* **2017**, *505*, 352−363.
(25) Zhuang, Y.-T.; Zhang, X.; Wang, D.-H.; Yu, Y.-L.; Wang, J.-H. Three-Dimensional Molybdenum Disulfide/graphene Hydrogel with Tunable Heterointerfaces for High Selective Hg(II) Scavenging. *J. Colloid Interface Sci.* **2018**, *514*, 715−722.
(26) Awad, F. S.; AbouZeid, K. M.; El-Maaty, W. M. A.; El-Wakil, A. M.; El-Shall, M. S. Efficient Removal of Heavy Metals from Polluted Water with High Selectivity for Mercury(II) by 2-Imino-4-thiobiuret−Partially Reduced Graphene Oxide (IT-PRGO). *ACS Appl. Mater. Interfaces* **2017**, *9* (39), 34230−34242.
(27) Yap, P. L.; Kabiri, S.; Tran, D. N. H.; Losic, D. Multifunctional Binding Chemistry on Modified Graphene Composite for Selective and Highly Efficient Adsorption of Mercury. *ACS Appl. Mater. Interfaces* **2019**, *11* (6), 6350−6362.
(28) Kabiri, S.; Tran, D. N. H.; Azari, S.; Losic, D. Graphene-Diatom Silica Aerogels for Efficient Removal of Mercury Ions from Water. *ACS Appl. Mater. Interfaces* **2015**, *7* (22), 11815−11823.
(29) Rahman, M. T.; Kabir, M. F.; Gurung, A.; Reza, K. M.; Pathak, R.; Ghimire, N.; Baride, A.; Wang, Z.; Kumar, M.; Qiao, Q. Graphene Oxide−Silver Nanowire Nanocomposites for Enhanced Sensing of Hg2+. *ACS Appl. Nano Mater.* **2019**, *2* (8), 4842−4851.
(30) Rodríguez-Mata, V.; González-Domínguez, J. M.; Benito, A. M.; Maser, W. K.; García-Bordejé, E. Reduced Graphene Oxide Aerogels with Controlled Continuous Microchannels for Environmental Remediation. *ACS Appl. Nano Mater.* **2019**, *2* (3), 1210−1222.
(31) Cui, H.; Qian, Y.; Li, Q.; Zhang, Q.; Zhai, J. Adsorption of Aqueous Hg(II) by a Polyaniline/attapulgite Composite. *Chem. Eng. J.* **2012**, *211*−*212*, 216−223.
(32) Fu, W.; Chen, H.; Yang, S.; Huang, W.; Huang, Z. Poly(diallyldimethylammonium-MoS4) Based Amorphous Molybdenum Sulphide Composite for Selectively Mercury Uptake from Wastewater across a Large pH Region. *Chemosphere* **2019**, *232*, 9−17.
(33) Ballav, N.; Das, R.; Giri, S.; Muliwa, A. M.; Pillay, K.; Maity, A. L-Cysteine Doped Polypyrrole (PPy@L-Cyst): A Super Adsorbent for the Rapid Removal of Hg+2 and Efficient Catalytic Activity of the Spent Adsorbent for Reuse. *Chem. Eng. J.* **2018**, *345*, 621−630.
(34) Feng, L.; Chen, W.-M.; Li, J.-L.; Day, G.; Drake, H.; Joseph, E.; Zhou, H.-C. Biological Antagonism Inspired Detoxification: Removal of Toxic Elements by Porous Polymer Networks. *ACS Appl. Mater. Interfaces* **2019**, *11* (15), 14383−14390.
(35) Shetty, D.; Boutros, S.; Eskhan, A.; De Lena, A. M.; Skorjanc, T.; Asfari, Z.; Traboulsi, H.; Mazher, J.; Raya, J.; Banat, F.; Trabolsi, A. Thioether-Crown-Rich Calix[4]arene Porous Polymer for Highly Efficient Removal of Mercury from Water. *ACS Appl. Mater. Interfaces* **2019**, *11* (13), 12898−12903.
(36) Song, J.; Kong, H.; Jang, J. Adsorption of Heavy Metal Ions from Aqueous Solution by Polyrhodanine-Encapsulated Magnetic Nanoparticles. *J. Colloid Interface Sci.* **2011**, *359* (2), 505−511.
(37) Tian, H.; He, J.; Hu, M. A Selectivity-Controlled Adsorbent of Molybdenum Disulfide Nanosheets Armed with Superparamagnetism for Rapid Capture of Mercury Ions. *J. Colloid Interface Sci.* **2019**, *551*, 251−260.
(38) He, F.; Wang, W.; Moon, J.-W.; Howe, J.; Pierce, E. M.; Liang, L. Rapid Removal of Hg(II) from Aqueous Solutions Using Thiol-Functionalized Zn-Doped Biomagnetite Particles. *ACS Appl. Mater. Interfaces* **2012**, *4* (8), 4373−4379.
(39) Yang, Z.; Li, H.; Liao, C.; Zhao, J.; Feng, S.; Li, P.; Liu, X.; Yang, J.; Shih, K. Magnetic Rattle-Type Fe_3O_4@CuS Nanoparticles as Recyclable Sorbents for Mercury Capture from Coal Combustion Flue Gas. *ACS Appl. Nano Mater.* **2018**, *1* (9), 4726−4736.
(40) Sun, Y.; Liu, Y.; Lou, Z.; Yang, K.; Lv, D.; Zhou, J.; Baig, S. A.; Xu, X. Enhanced Performance for Hg(II) Removal Using Biomaterial (CMC/gelatin/starch) Stabilized FeS Nanoparticles: Stabilization Effects and Removal Mechanism. *Chem. Eng. J.* **2018**, *344*, 616−624.
(41) Lone, S.; Yoon, D. H.; Lee, H.; Cheong, I. W. Gelatin−chitosan Hydrogel Particles for Efficient Removal of Hg(II) from Wastewater. *Environ. Sci. Water Res. Technol.* **2019**, *5* (1), 83−90.
(42) Jiang, J.; Zhang, Q.; Zhan, X.; Chen, F. A Multifunctional Gelatin-Based Aerogel with Superior Pollutants Adsorption, Oil/water Separation and Photocatalytic Properties. *Chem. Eng. J.* **2019**, *358*, 1539−1551.
(43) Li, X.; Cao, W.; Liu, Y.; Zeng, G.; Zeng, W.; Qin, L.; Li, T. Property Variation of Magnetic Mesoporous Carbon Modified by Aminated Hollow Magnetic Nanospheres: Synthesis, Characterization, and Sorption. *ACS Sustainable Chem. Eng.* **2017**, *5* (1), 179−188.
(44) Kabiri, S.; Tran, D. N. H.; Cole, M. A.; Losic, D. Functionalized Three-Dimensional (3D) Graphene Composite for High Efficiency Removal of Mercury. *Environ. Sci. Water Res. Technol.* **2016**, *2* (2), 390−402.
(45) Inonu, Z.; Keskin, S.; Erkey, C. An Emerging Family of Hybrid Nanomaterials: Metal−Organic Framework/Aerogel Composites. *ACS Appl. Nano Mater.* **2018**, *1* (11), 5959−5980.
(46) Štandeker, S.; Novak, Z.; Knez, Ž. Adsorption of Toxic Organic Compounds from Water with Hydrophobic Silica Aerogels. *J. Colloid Interface Sci.* **2007**, *310* (2), 362−368.
(47) García-González, C. A.; Budtova, T.; Durães, L.; Erkey, C.; Del Gaudio, P.; Gurikov, P.; Koebel, M.; Liebner, F.; Neagu, M.; Smirnova, I. An Opinion Paper on Aerogels for Biomedical and Environmental Applications. *Molecules* **2019**, *24* (9), 1815.
(48) Vareda, J. P.; Valente, A. J. M.; Durães, L. Heavy Metals in Iberian Soils: Removal by Current Adsorbents/amendments and Prospective for Aerogels. *Adv. Colloid Interface Sci.* **2016**, *237*, 28−42.

DOI: 10.1021/acsanm.9b01903
ACS Appl. Nano Mater. 2020, 3, 195−206

(49) Maleki, H. Recent Advances in Aerogels for Environmental Remediation Applications: A Review. *Chem. Eng. J.* **2016**, *300*, 98−118.
(50) Ali, Z.; Khan, A.; Ahmad, R. The Use of Functionalized Aerogels as a Low Level Chromium Scavenger. *Microporous Mesoporous Mater.* **2015**, *203*, 8−16.
(51) Maleki, H.; Hüsing, N. Aerogels as Promising Materials for Environmental remediation—A Broad Insight into the Environmental Pollutants Removal through Adsorption and (Photo)catalytic Processes. In *New Polymer Nanocomposites for Environmental Remediation*; Elsevier: 2018; pp 389−436.
(52) Kalmár, J.; Kéri, M.; Erdei, Z.; Bányai, I.; Lázár, I.; Lente, G.; Fábián, I. The Pore Network and the Adsorption Characteristics of Mesoporous Silica Aerogel: Adsorption Kinetics on a Timescale of Seconds. *RSC Adv.* **2015**, *5* (130), 107237−107246.
(53) Veres, P.; Kéri, M.; Bányai, I.; Lázár, I.; Fábián, I.; Domingo, C.; Kalmár, J. Mechanism of Drug Release from Silica-Gelatin aerogel—Relationship between Matrix Structure and Release Kinetics. *Colloids Surf., B* **2017**, *152*, 229−237.
(54) Veres, P.; López-Periago, A. M.; Lázár, I.; Saurina, J.; Domingo, C. Hybrid Aerogel Preparations as Drug Delivery Matrices for Low Water-Solubility Drugs. *Int. J. Pharm.* **2015**, *496* (2), 360−370.
(55) Lázár, I.; Fábián, I. A Continuous Extraction and Pumpless Supercritical CO_2 Drying System for Laboratory-Scale Aerogel Production. *Gels* **2016**, *2* (4), 26.
(56) Maleki, H.; Whitmore, L.; Hüsing, N. Novel Multifunctional Polymethylsilsesquioxane−silk Fibroin Aerogel Hybrids for Environmental and Thermal Insulation Applications. *J. Mater. Chem. A* **2018**, *6* (26), 12598−12612.
(57) Maleki, H.; Montes, S.; Hayati-Roodbari, N.; Putz, F.; Huesing, N. Compressible, Thermally Insulating, and Fire Retardant Aerogels through Self-Assembling Silk Fibroin Biopolymers Inside a Silica Structure—An Approach towards 3D Printing of Aerogels. *ACS Appl. Mater. Interfaces* **2018**, *10* (26), 22718−22730.
(58) Burgess, D. J.; Carless, J. E. Microelectrophoretic Studies of Gelatin and Acacia for the Prediction of Complex Coacervation. *J. Colloid Interface Sci.* **1984**, *98* (1), 1−8.
(59) Limousin, G.; Gaudet, J.-P.; Charlet, L.; Szenknect, S.; Barthès, V.; Krimissa, M. Sorption Isotherms: A Review on Physical Bases, Modeling and Measurement. *Appl. Geochem.* **2007**, *22* (2), 249−275.
(60) Cheesman, B. V.; Arnold, A. P.; Rabenstein, D. L. Nuclear Magnetic Resonance Studies of the Solution Chemistry of Metal Complexes. 25. Hg(thiol)3 Complexes and HG(II)-Thiol Ligand Exchange Kinetics. *J. Am. Chem. Soc.* **1988**, *110* (19), 6359−6364.
(61) Hahne, H. C. H.; Kroontje, W. Significance of pH and Chloride Concentration on Behavior of Heavy Metal Pollutants: Mercury(II), Cadmium(II), Zinc(II), and Lead(II)1. *J. Environ. Qual.* **1973**, *2* (4), 444.
(62) Gupta, N. K.; Gupta, A. 2D and 3D Carbon-Based Adsorbents for an Efficient Removal of HgII Ions: A Review. *FlatChem.* **2018**, *11*, 1−14.
(63) Adam, M.; Fietzek, P.; Deyl, Z.; Rosmus, J.; Kuhn, K. Investigations on the Reaction of Metals with Collagen in Vivo. 3. The Effect of Bismuth, Copper and Mercury Compounds. *Eur. J. Biochem.* **1968**, *3* (4), 415−418.
(64) Anderson, D. H.; Murphy, J. J.; White, W. W. Gelatin as a Matrix for a Mercury Reference Material. *Anal. Chem.* **1972**, *44* (12), 2099−2100.
(65) Wang, Y.; Tang, M.; Shen, H.; Che, G.; Qiao, Y.; Liu, B.; Wang, L. Recyclable Multifunctional Magnetic Mesoporous Silica Nanocomposite for Ratiometric Detection, Rapid Adsorption, and Efficient Removal of Hg(II). *ACS Sustainable Chem. Eng.* **2018**, *6* (2), 1744−1752.

DOI: 10.1021/acsanm.9b01903
ACS Appl. Nano Mater. 2020, 3, 195−206